

False Negative Reduction in Semantic Segmentation under Domain Shift using Depth Estimation

Kira Maag
Ruhr University Bochum, Germany
kira.maag@rub.de

Matthias Rottmann
University of Wuppertal, Germany
rothmann@uni-wuppertal.de

Abstract—State-of-the-art deep neural networks demonstrate outstanding performance in semantic segmentation. However, their performance is tied to the domain represented by the training data. Open world scenarios cause inaccurate predictions which is hazardous in safety relevant applications like automated driving. In this work, we enhance semantic segmentation predictions using monocular depth estimation to improve segmentation by reducing the occurrence of non-detected objects in presence of domain shift. To this end, we infer a depth heatmap via a modified segmentation network which generates foreground-background masks, operating in parallel to a given semantic segmentation network. Both segmentation masks are aggregated with a focus on foreground classes (here road users) to reduce false negatives. To also reduce the occurrence of false positives, we apply a pruning based on uncertainty estimates. Our approach is modular in a sense that it post-processes the output of any semantic segmentation network. In our experiments, we observe less non-detected objects of most important classes and an enhanced generalization to other domains compared to the basic semantic segmentation prediction.

I. INTRODUCTION

Semantic image segmentation aims at segmenting objects in an image by assigning each pixel to a class within a predefined set of semantic classes. Thereby, semantic segmentation provides comprehensive and precise information about the given scene. This is particularly desirable in safety relevant applications like automated driving. In recent years, deep neural networks (DNNs) have demonstrated outstanding performance on this task [1], [2]. However, DNNs are usually trained on a specific dataset (source domain) and often fail to function properly on unseen data (target domain) due to a domain gap. An example of this behavior is shown in Figure 1. The DNN is trained on urban traffic data from Germany, Cityscapes dataset [3], and incorrectly predicts the unseen animals in Indian street scenes [4] as person, nature or fence. This is critical since potential hazardous situations are underestimated due to the prediction of non-dynamic classes.

Unsupervised domain adaptation is an approach overcoming this issue. The idea is to train a DNN on labeled source domain data and jointly on unlabeled target data adapting the source domain distribution to the target one [5]. As target data is not always available for training, the recent research has also been devoted to *domain generalization* resolving this limitation. The model is trained solely on source data without access to target data using a shared representation across multiple source domains improving the robustness to unseen domains [6], [7].



Fig. 1. Example image of the India Driving dataset. *Left*: Ground truth pixels of classes humans/animals colored in red and vehicles in blue. *Right*: Semantic segmentation for the mentioned classes.

In real-world applications, domain gaps may occur due to shifts in location, time and other environmental parameters. This causes domain shift on both, foreground and background classes. For many years, computer vision has used the decomposition into *things* – countable objects such as persons, animals, vehicles – and *stuff* – regions with similar texture or material like sky, road, nature, buildings – which is analogous to the foreground-background splitting [8], [9]. The appearance of foreground objects may vary over time or due to a change of location and the same applies to the environment (background). Figure 1 gives an example for the lack of generalization, i.e., the DNN is trained only on street scenes in German cities resulting in defective behavior on the unseen Indian road scenes. On the one hand, using semantic segmentation in open world scenarios, such as in automated driving, the appearance of objects that do not belong to any of the semantic classes the DNN has been trained on (like animals) may cause defective predictions [10]. On the other hand, even objects of known classes can change their appearance, leading to erroneous predictions. For these reasons, the generalization of DNNs bridging the domain gap is of highest interest. In applications like automated driving, the foreground class is of particular interest due to its dynamical behavior. Especially in presence of domain gaps, the detection performance w.r.t. these object classes can decrease significantly. To this end, we propose a false negative reduction method which is robust against domain shift.

In this work, we introduce a domain generalization method reducing false negatives of important classes in semantic segmentation in the area of automated driving. Our approach serves as a post-processing step applicable to any semantic segmentation network. An overview is shown in Figure 2. Our method consists of two branches. The *image segmentation*

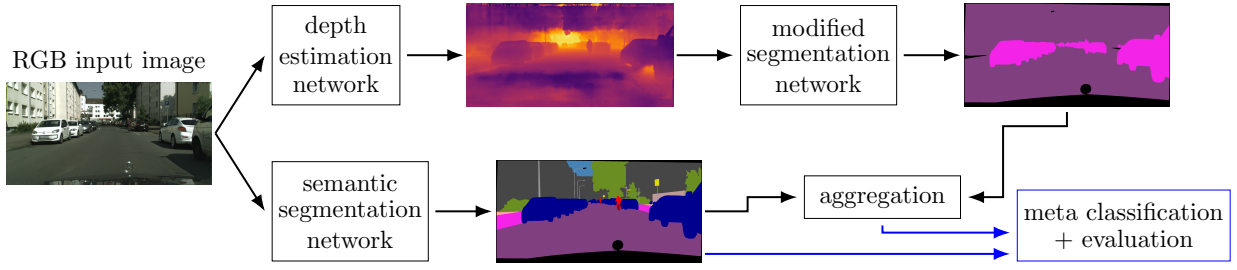


Fig. 2. Overview of our method. The input image is fed into a semantic segmentation network (bottom branch) and in parallel into a depth estimation network (top branch). The resulting depth heatmap is passed to our modified segmentation network which predicts a foreground-background segmentation. This prediction is aggregated with the semantic segmentation and finally, meta classification is applied to reduce false positive segments.

branch is a semantic segmentation inference and the *depth segmentation branch* feeds the same RGB input image into a depth estimation network. The goal of depth estimation is to obtain a representation of the spatial structure of a given scene. The resulting depth heatmap is passed to a modified segmentation network which predicts foreground-background segmentation. The architecture of this network may be based on the architecture of the semantic segmentation network, but can be chosen independently. The foreground class consists of the most important classes in street scene segmentation, humans and vehicles. In the *fusion* step, the semantic segmentation and the foreground-background prediction are aggregated obtaining several segments (connected components of pixels belonging to the same class) per foreground class. As a result of combining the two masks, we detect overlooked segments of the basic semantic segmentation network on the source dataset as well as under domain shift using the depth information for domain generalization. However, the increased sensitivity towards finding foreground objects may result in an overproduction of false positive segments. To overcome this, we utilize so-called meta classification as *false positive pruning*, introduced for semantic segmentation in [11], [12] and for instance segmentation in [13]. It tackles the task of predicting whether a segment intersects with ground truth or not which is measured by a commonly used performance measure, the intersection over union [14]. Meta classification is used after the fusion step to also achieve a high precision rate [15], [16]. Moreover, to gain a further performance boost, the meta classifier, which is trained only on the source domain, can be fine-tuned on a small amount of the respective target domain (lightweight domain adaptation).

We only assume input data as well as a trained semantic segmentation and a depth estimation network. Due to the modularity of our method, we can set up our model based on these assumptions. In our tests, we employ two semantic segmentation [1], [17] and two depth estimation networks [18], [19] applied to four datasets, i.e., Cityscapes [3] as source domain and A2D2 [20], LostAndFound [10] as well as India Driving [4] as target domains. The application of these widely differing datasets is intended to demonstrate the domain generalization and error reduction capability of our approach. The source code of our method is publicly available at

<http://github.com/kmaag/FN-Reduction-using-Depth> Our contributions are summarized as follows:

- We introduce a modified segmentation network which is fed with depth heatmaps and outputs foreground-background segmentation masks. The depth information enhances the robustness of the prediction in the presence of domain shift.
- We combine these foreground-background segmentation masks with semantic segmentation masks to detect possible overlooked segments (by the semantic segmentation network) of the most important classes. In addition, we perform meta classification to prune false positive segments.
- For the first time, we demonstrate successfully that depth information improves a semantic segmentation performance in a post-processing step (independently of the choice of semantic segmentation network). We compare the performance of our method with basic semantic segmentation performance on several datasets with domain gap, i.e., different semantic classes and/or environments obtaining area under precision-recall curve values of up to 97.08% on source domain and 93.83% under domain shift.

The paper is structured as follows. In Section II, we discuss the related work. Our approach is introduced in Section III including the modified segmentation network, the aggregation of network predictions and meta classification. The numerical results are shown in Section IV.

II. RELATED WORK

In this section, we first discuss related methods improving robustness of DNNs under domain shift as well as false negative reduction approaches. Thereafter, we present works that use depth information to enhance semantic segmentation prediction.

a) *Robustness under Domain Shift*: Unsupervised domain adaptation is often used to strengthen the robustness of DNNs bridging domain gaps [5]. The DNN is trained with source data (labeled) and target data (unlabeled and different from source dataset) to align the target domain’s distributions. In [21], this problem is tackled by a generative adversarial network which translates the target domain into the source

domain before predicting semantic segmentation. Monocular depth estimation is used in [22], [23] to improve the prediction performance under domain shift. However, target data from various environments is not always available during the training process. To overcome this limitation, research on domain generalization has recently gained attention, using only source data to train the model.

Synthetic to real domain generalization offers a possibility to exploit the advantage of the availability of synthetic data. In [24], the synthetically trained network is encouraged to maintain similar representations as the ImageNet pre-trained model. In other works, style-diversified samples [25] or web-crawled images [26] are utilized for improving the representational consistency between synthetic and real-world for the sake of generalizable semantic segmentation. The model presented in [6] is trained on multiple source domains (synthetic and real) to generalize to unseen data domains. The variety of contents and styles from ImageNet is leveraged in [7] to learn domain-generalized semantic features. In [27], an instance selective whitening loss is introduced to disentangle the domain-specific style and domain-invariant content to remove only the style information causing domain shift.

In contrast to domain adaptation, our method does not require target domain data for training. The presented domain generalization approaches use a great amount of source domain data and/or modify the training process of the semantic segmentation network while we only consider depth information for domain generalization and are independent of the semantic segmentation network due to modularity.

b) False Negative Reduction in Semantic Segmentation: Reducing false negatives, i.e., obtaining a higher recall rate, is often achieved in semantic segmentation by modifying the loss function. In [28], a higher recall rate for a real-time DNN is obtained by modifying the loss function, classifier and decision rule. A similar approach presented in [29] considers an importance-aware loss function to improve a network's reliability. To reduce false negative segments of minority classes, differences between the Bayes and the Maximum Likelihood decision rule are exploited introducing class priors that assign larger weight to underrepresented classes [15]. Since minority classes are not necessarily hard to predict, leading to the prediction of many false positives, a hard-class mining loss is introduced in [30] by redesigning the cross entropy loss to dynamically weight the loss for each class based on instantaneous recall. In [31], false negative pixels in semi-supervised semantic segmentation are reduced by using the pixel-level ℓ_2 loss and the pixel contrastive loss.

While the presented approaches modify the training process and/or the decision rule, we propose a post-processing method. For the first time, we present a false negative reduction approach which overcomes domain gaps using depth information. The only work [16] which also uses depth heatmaps addressing the recall rate improvement works on video instance segmentation.

c) Improving Segmentation using Depth Estimation: The predictions of semantic segmentation and depth estimation

are improved in previous works using joint network architectures sharing information for both tasks [32], [33]. Furthermore, approaches are introduced where information of one task enhance the prediction quality of the other task. The semantic segmentation task is improved in [34] by an encoder consisting of two network branches which extract features from depth and RGB images simultaneously. In [35], RGB-D data is also fed into a network that extracts both RGB and depth features in parallel for semantic segmentation prediction (and object detection). Contrary, a single shared encoder is used in [36] to enhance performance for a supervised task, here semantic segmentation, which obtains information of two self-supervised tasks (colorization and depth prediction) exploiting unlabeled data. In [37], a semantic segmentation network is pre-trained for depth prediction to serve as a powerful proxy for learning visual representations. In addition to learning features from depth information, a student-teacher framework is considered in [38] to select the most helpful samples to annotate for semantic segmentation.

In comparison to the described methods for improving semantic segmentation prediction via depth estimation, our approach does not modify the network architecture. Instead, our foreground-background prediction and the aggregation serve as post-processing steps, i.e., any semantic segmentation network can be used and thus, the network architecture is not altered. Contrary to the domain generalization and false negative reduction approaches, we consider the advantages of depth estimation to enhance the prediction performance under domain shift.

III. METHOD DESCRIPTION

Our method is composed of two branches, i.e., the image segmentation and depth segmentation branch, see Figure 2. The outputs of both streams are aggregated to detect segments overlooked by the basic semantic segmentation network. As many false positive segments can be generated by the fusion, false positive pruning is applied in an additional post-processing step.

A. Foreground-Background Segmentation

In this section, we introduce our modified segmentation network for foreground-background segmentation. We assume that a depth estimation (and a semantic segmentation ground truth) is available for each input image. Our approach is a post-processing step and independent of the choice of the depth estimation (and the semantic segmentation) network. The basis for the modified network can be any standard semantic segmentation network. However, instead of feeding an RGB image into the network a depth estimation heatmap is used and the semantic space is composed of only two classes - foreground and background.

The binarization into foreground and background is adapted from the *thing* and *stuff* decomposition in the computer vision field like in panoptic segmentation. Using automated driving as example application, things are countable objects such as persons, animals, cars or bicycles. The stuff classes consist of

amorphous regions of similar texture or material such as sky, road, nature or buildings. Note, the idea of things and stuff also exists in other application areas like robot navigation. The thing classes receive the dominant share of attention in computer vision tasks such as object detection and instance segmentation. In automated driving, the foreground class is of particular interest due to its dynamical behavior.

B. Aggregation of Predictions

From the first branch, we obtain a semantic segmentation prediction, i.e., a pixel-wise classification of image content. The DNN provides for each pixel z a probability distribution $f_z(y|x)$ over a prescribed label space $y \in \mathcal{C} = \{y_1, \dots, y_c\}$ with c different class labels, given an input image x . The predicted class for each pixel z is computed by the maximum a-posteriori principle

$$\hat{y}_z(x) = \arg \max_{y \in \mathcal{C}} f_z(y|x). \quad (1)$$

The second branch provides a foreground-background segmentation. Given the same input image x , we obtain for each pixel z the probability of being a foreground pixel $g_z(x) \in [0, 1]$ considering a binary classification problem. The predicted segmentations are aggregated pixel-wise resulting in a combined prediction with the class label background y_0 or a foreground class label $y \in \tilde{\mathcal{C}} \subset \mathcal{C}$ per pixel. For this, we split the label space into foreground class labels $\tilde{\mathcal{C}} = \{y_1, \dots, y_{\tilde{c}}\}$, $\tilde{c} < c$, and background class labels $\{y_{\tilde{c}+1}, \dots, y_c\}$ with $y_0 = \mathcal{C} \setminus \tilde{\mathcal{C}}$. The combination is defined per pixel by

$$\hat{s}_z(x) = \begin{cases} \hat{y}_z(x), & \text{if } \hat{y}_z(x) \in \tilde{\mathcal{C}} \\ \arg \max_{y \in \tilde{\mathcal{C}}} f_z(y|x), & \text{if } g_z(x) > 0.5 \wedge \hat{y}_z(x) \notin \tilde{\mathcal{C}} \\ y_0, & \text{else} \end{cases} \quad (2)$$

If the semantic segmentation network predicts a foreground class or the foreground-background network predicts foreground, the pixel is considered as foreground and assigned to the foreground class $y \in \tilde{\mathcal{C}}$ of the semantic segmentation with the highest probability. Otherwise, the pixel is assigned to the class background. Moreover, $\hat{\mathcal{S}}_x = \{\hat{s}_z(x) | z \in x\}$ denotes the combined segmentation consisting of foreground classes and the background class.

C. Meta Classification

The combination of the semantic segmentation and the foreground-background prediction can increase the number of false positives. For this reason, we apply meta classification [11] as false positive pruning step using uncertainty measures. The degree of randomness in semantic segmentation prediction $f_z(y|x)$ is quantified by (pixel-wise) dispersion measures, like the entropy. To obtain segment-wise features characterizing uncertainty of a given segment from these pixel-wise dispersion measures, we aggregate them over segments by average pooling. In addition, we hand-craft features based on object's geometry like the segment size or the geometric center obtaining uncertainty information. These hand-crafted

measures form a structured dataset where the rows correspond to predicted segments and the columns to features. A detailed description of these hand-crafted features can be found in [Appendix A](#).

To determine if a predicted segment is a false positive, i.e., has no overlap with a ground truth segment of a foreground class, we consider the intersection over union (IoU), a typical performance measure of segmentation networks with respect to the ground truth. Meta classification tackles the task of classifying between $IoU = 0$ (false positive) and $IoU > 0$ (true positive) for all predicted segments. If a segment is predicted to be a false positive, it is no longer considered as a foreground segment but as background. We perform meta classification using our structured dataset as input. Note, these hand-crafted measures are computed without the knowledge of the ground truth data. To train the classifier, we use gradient boosting [39] that outperforms linear models and shallow neural networks as shown in [13]. We study to which extent our aggregated prediction followed by meta classification improves the detection performance for important classes compared to basic semantic segmentation.

IV. EXPERIMENTS

In this section, we first present the experimental setting and then demonstrate the performance improvements of our method compared to the basic semantic segmentation network in terms of false negative reduction overcoming the domain gap.

A. Experimental Setting

a) *Datasets*: We perform our tests on four datasets for semantic segmentation in street scenes considering Cityscapes [3] as source domain and A2D2 [20], LostAndFound [10] as well as India Driving (IDD) [4] as target domains. The training/validation split of Cityscapes consists of 2,975/500 images from dense urban traffic in 18/3 different German towns, respectively. Thus, our foreground class consists of all road user classes, i.e., human (person and rider) and vehicle (car, truck, bus, train, motorcycle and bicycle) and the background of categories flat, construction, object, nature and sky. From the A2D2 dataset, we sample 500 images out of 23 image sequences for our tests covering urban, highways and country roads in three cities. This variety of environments is not included in the Cityscapes dataset resulting in a domain shift in the background. The validation set of LostAndFound containing 1,203 images is designed for detecting small obstacles on the road in front of the ego-car. This causes a foreground domain shift as these objects are not contained in the semantic space of Cityscapes. We use 538 frames of the IDD dataset which contains unstructured environments of Indian roads inducing a domain shift in both, foreground and background. The latter is caused by, for example, the diversity of ambient conditions and ambiguous road boundaries. The foreground domain shift occurs as the IDD dataset consists of two more relevant foreground classes

(animals and auto rickshaws) and the Cityscapes foreground objects differ significantly.

b) *Networks*: We consider the state-of-the-art DeepLabv3+ network [1] with WideResNet38 [40] as backbone and the more lightweight (and thus weaker) DualGCNet [17] with ResNet50 [41] backbone for semantic segmentation. Both DNNs are trained on the Cityscapes dataset achieving *mean IoU* ($mIoU$) values of 90.29% for DeepLabv3+ and 79.68% for DualGCNet on the Cityscapes validation set. For depth estimation trained on the KITTI dataset [42], we use the supervised depth estimation network BTS [19] with DenseNet-161 [43] backbone obtaining a *relative absolute error* on the KITTI validation set of 0.090 and the unsupervised Monodepth2 [18] with ResNet18 backbone achieving 0.106 *relative absolute error*. Our modified segmentation network is based on the DeepLabv3+ architecture with WideResNet38 backbone having high predictive power and is fed with depth estimation heatmaps of the Cityscapes dataset predicted by the BTS network and Monodepth2, respectively. We train this network on the training split of the Cityscapes dataset and use the binarized (into foreground and background) semantic segmentation ground truth to compare our results with the basic semantic segmentation network which is also trained on Cityscapes. For the BTS network a validation $mIoU$ of 88.34% is obtained and for Monodepth2 of 85.12%.

c) *Evaluation Metrics*: Meta classification provides a probability of observing a false positive segment and such a predicted false positive segment is considered as background. We threshold on this probability with 101 different values $h \in H = \{0.00, 0.01, \dots, 0.99, 1.00\}$. For each threshold, we calculate the number of true positive, false positive and false negative foreground segments resulting in precision ($prec(h)$) and recall ($rec(h)$) values on segment-level depended of h . The degree of separability is then computed as the area under precision recall curve ($AUPRC$) by thresholding the meta classification probability. In addition, we compute the recall rate at 80% precision rate (REC_{80}) for the evaluation. Furthermore, we consider the segment-wise F_1 score which is defined by $F_1(h) = 2 \cdot prec(h) \cdot rec(h) / (prec(h) + rec(h))$. To obtain an evaluation metric independent of the meta classification threshold h , we calculate the averaged F_1 score $\bar{F}_1 = \frac{1}{|H|} \sum_{h \in H} F_1(h)$ and the optimal F_1 score $F_1^* = \max_{h \in H} F_1(h)$. For a detailed description of these metrics see Appendix B.

B. Numerical Results

a) *Results on the Source Domain*: First, we study the predictive power of the meta classifier trained on the Cityscapes (validation) dataset using a train/test splitting of 80%/20% shuffling 5 times, such that all segments are a part of the test set. We use meta classification to prune possible false positive segments that are falsely predicted as foreground segments. For the comparison of basic semantic segmentation performance with our approach, meta classifiers are trained on the predicted foreground segments, respectively. These

| | $AUPRC$ | \bar{F}_1 | F_1^* | REC_{80} |
|--------------|--------------|--------------|--------------|--------------|
| DeepLabv3+ | 94.26 | 90.61 | 94.69 | 94.49 |
| + BTS | 97.07 | 90.21 | 95.80 | 97.15 |
| + Monodepth2 | 97.08 | 90.03 | 95.73 | 97.15 |
| DualGCNet | 91.85 | 88.68 | 92.77 | 92.18 |
| + BTS | 95.90 | 87.92 | 94.66 | 95.88 |
| + Monodepth2 | 95.63 | 87.94 | 94.58 | 95.66 |

TABLE I
PERFORMANCE RESULTS FOR THE CITYSCAPES DATASET FOR THE BASIC SEMANTIC SEGMENTATION PREDICTION VS. OUR APPROACH, I.E., THE DEEPLABV3+/DUALGCNET PREDICTION AGGREGATED WITH FOREGROUND-BACKGROUND PREDICTION USING BTS OR MONODEPTH2.

| | Cityscapes | A2D2 | IDD |
|--------------|------------|----------|----------|
| DeepLabv3+ | 90.29% | 61.98% | 57.26% |
| + BTS | -4.72 pp | -2.87 pp | -1.59 pp |
| + Monodepth2 | -5.97 pp | -4.84 pp | -3.99 pp |
| DualGCNet | 79.68% | 23.76% | 45.79% |
| + BTS | -3.99 pp | +0.12 pp | -1.03 pp |
| + Monodepth2 | -5.09 pp | -0.49 pp | -3.12 pp |

TABLE II
 $mIoU$ RESULTS FOR BOTH SEMANTIC SEGMENTATION NETWORKS AND THE DIFFERENCE TO OUR APPROACH. A HIGHER $mIoU$ VALUE CORRESPONDS TO BETTER PERFORMANCE.

classifiers achieve test classification $AUROC$ values between 94.68% and 99.14%. The $AUROC$ (area under receiver operating characteristic curve) is obtained by varying the decision threshold in a binary classification problem, here for the decision between $IoU = 0$ and > 0 . The influence of meta classification on the performance is studied in Appendix C.

We compare the detection performances which are shown in Table I using presented evaluation metrics. We observe that our method obtain higher $AUPRC$, F_1^* and REC_{80} values than the semantic segmentation prediction. Note, there is no consistency on which depth estimation network yields more enhancement. In particular, we reduce the number of non-detected segments of foreground classes. In Figure 3 (left), the highest recall values of the semantic segmentation predictions are shown, i.e., no segments are deleted using meta classification. For our method, we use the meta classification threshold where the precision of our method is equal to that of the baseline. As a consequence, for the identical precision values we observe an increase in recall by up to 2.71 percent points (pp) for the Cityscapes dataset. In Appendix D, more numerical results evaluated on individual foreground classes are presented.

The $mIoU$ is the commonly used performance measure for semantic segmentation. To compute the $mIoU$ for the aggregated prediction \hat{S}_x , we have to fill the background values as they are ignored up to now. Similar to how we obtain the foreground class during the combination, we assign to every background pixel the background class $y \in C \setminus \hat{C}$ of the semantic segmentation with the highest probability. The results for semantic segmentation prediction and the difference to our aggregated predictions are shown in the Cityscapes column of Table II. We perform slightly worse in the overall performance accuracy ($mIoU$) as the foreground-background masks are location-wise less accurate than the segmentation masks, see Figure 4. Nonetheless, we detect foreground objects, here road users, that are overlooked by the semantic segmentation

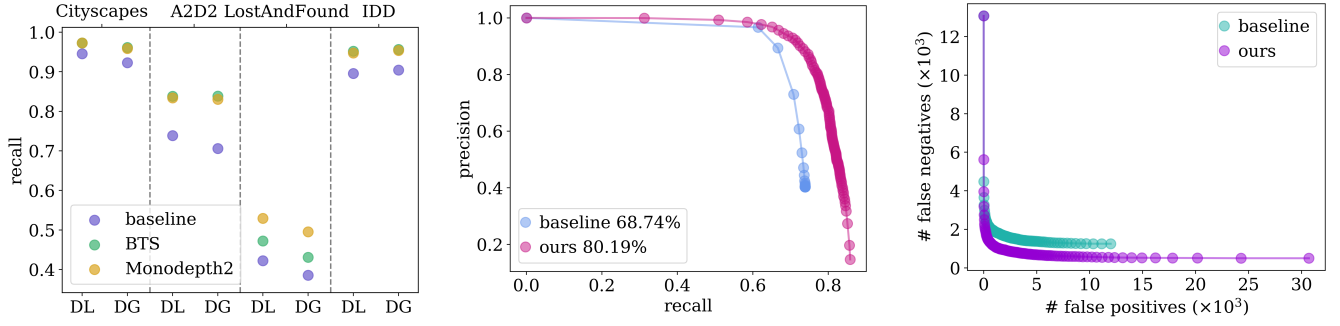


Fig. 3. *Left*: The recall values under the assumption of same precision values for all datasets and networks. We distinguish the performance for the DeepLabv3+ (DL) and the DualGCNet (DG) semantic segmentation networks whose predictions serve as baselines. We compare these with our approach using the BTS and the Monodepth2 depth estimation network, respectively. *Center*: Precision-recall curves for the A2D2 dataset, the DeepLabv3+ and BTS networks. *Right*: Number of false positive vs. false negative segments for different meta classification thresholds for the IDD dataset, the DualGCNet and BTS networks using 20% of this dataset for fine-tuning.

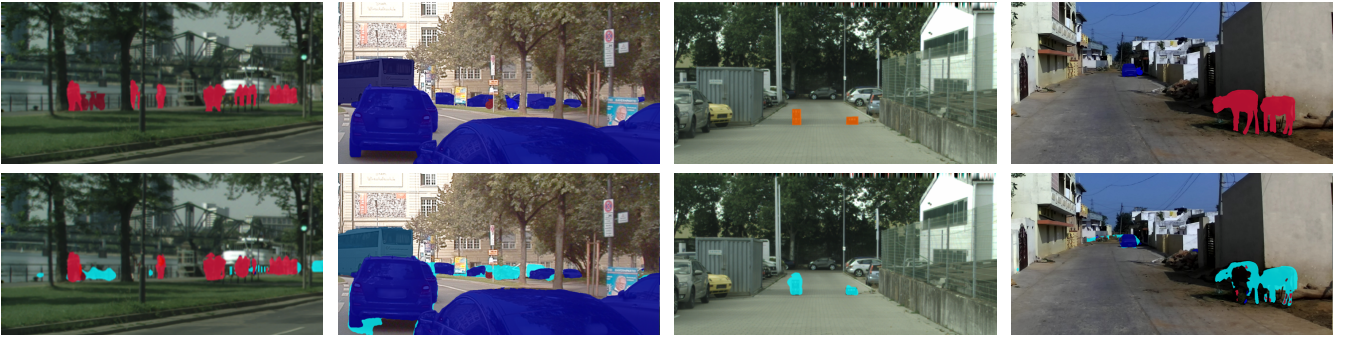


Fig. 4. Examples for segments that are overlooked by the basic semantic segmentation network and detected by our approach for Cityscapes (DualGCNet, BTS, *left*), A2D2 (DeepLabv3+, BTS, *center left*), LostAndFound (DeepLabv3+, Monodepth2, *center right*) and IDD dataset (DeepLabv3+, BTS, *right*). *Top*: Ground truth images including only the labels of foreground classes. *Bottom*: Basic semantic segmentation prediction in typical Cityscapes colors for foreground segments (shades of blue and red) as well as the foreground prediction of our modified segmentation network (cyan).

network (for example, see the bicycle in Figure 4 (left)).

b) Results under Domain Shift: In this section, we study the false negative reduction for the A2D2, LostAndFound and IDD datasets under domain shift from the source domain Cityscapes. As mentioned above, since the semantic segmentation networks as well as the modified segmentation networks are trained on the Cityscapes dataset, we train also the meta classification model on this dataset using all predicted segments. We obtain meta classification test *AUROC* values up to 93.12% for A2D2, 91.65% for LostAndFound and 93.97% for IDD.

We compare the performance of our approach with the semantic segmentation prediction by computing the evaluation metrics, results are given in Table III.

The performance metrics are greatly increased by our method demonstrating that our approach is more robust to domain shift. Noteworthy, we outperform the stronger DeepLabv3+ network in all cases. Example curves are presented in Figure 3 (center) for the A2D2 dataset where an *AUPRC* enhancement of 11.45 pp is obtained. Our precision-recall curve is entirely above the baseline. In particular, for identical precision values, we obtain an increase in recall by up

to 13.24 pp, i.e., reduce the number of false negative segments, as also shown in Figure 3 (left). Examples for detected segments that are missed by the semantic segmentation network are given in Figure 4 for all datasets. Hence, our method detect segments of well-trained classes, i.e., the overlooked bicycle in the Cityscapes dataset or various cars in A2D2. Moreover, we bridge the domain gap as we find small obstacles (LostAndFound) and animals (IDD) that are not part of the Cityscapes dataset and thus, are not included in the semantic space for training. In Appendix D, more numerical results evaluated on individual foreground classes are presented.

In Table II, the differences between the *mIoU* values are evaluated on the Cityscapes classes. For the A2D2 dataset, the classes are mapped to the Cityscapes ones and for the IDD dataset, we treat the additional classes animal as human and auto rickshaw as car. For the LostAndFound, an evaluation is not possible as it contains only labels for the road and the small obstacles which do not fit into the semantic space. With one positive exception, we are slightly worse in overall accuracy performance. On the one hand, the images in Figure 4 demonstrate why we decrease the accuracy slightly as the predictions and in particular, the segment boundaries are

| | A2D2 | | | | LostAndFound | | | | IDD | | | |
|--------------|--------------|--------------|--------------|--------------|--------------|--------------|--------------|--------------|--------------|--------------|--------------|--------------|
| | $AUPRC$ | \bar{F}_1 | F_1^* | REC_{80} | $AUPRC$ | \bar{F}_1 | F_1^* | REC_{80} | $AUPRC$ | \bar{F}_1 | F_1^* | REC_{80} |
| DeepLabv3+ | 68.74 | 52.72 | 76.36 | 70.80 | 40.05 | 50.27 | 53.06 | 39.40 | 84.11 | 69.19 | 87.79 | 88.52 |
| + BTS | 80.19 | 66.96 | 80.46 | 77.17 | 46.18 | 51.08 | 57.80 | 45.06 | 93.86 | 78.48 | 91.75 | 93.26 |
| + Monodepth2 | 80.01 | 66.77 | 80.72 | 77.15 | 51.67 | 54.15 | 60.41 | 48.07 | 93.35 | 76.69 | 91.45 | 92.86 |
| DualGCNet | 48.64 | 27.93 | 65.48 | 58.67 | 36.80 | 45.85 | 50.21 | 36.08 | 84.59 | 66.40 | 87.37 | 88.20 |
| + BTS | 42.16 | 36.27 | 51.22 | 26.90 | 42.34 | 47.27 | 53.59 | 40.12 | 92.23 | 71.85 | 89.78 | 92.53 |
| + Monodepth2 | 49.03 | 39.01 | 57.26 | 19.29 | 47.92 | 49.11 | 57.06 | 44.16 | 92.39 | 73.17 | 89.82 | 92.23 |

TABLE III

PERFORMANCE RESULTS FOR THE BASIC SEMANTIC SEGMENTATION PREDICTION VS. OUR APPROACH.

| | | A2D2 | | | | LostAndFound | | | | IDD | | | |
|----------------------------|-----|--------------|--------------|--------------|--------------|--------------|--------------|--------------|--------------|--------------|--------------|--------------|--------------|
| | | $AUPRC$ | \bar{F}_1 | F_1^* | REC_{80} | $AUPRC$ | \bar{F}_1 | F_1^* | REC_{80} | $AUPRC$ | \bar{F}_1 | F_1^* | REC_{80} |
| DeepLabv3+ + BTS | 0% | 80.19 | 66.96 | 80.46 | 77.17 | 46.18 | 51.08 | 57.80 | 45.06 | 93.86 | 78.48 | 91.75 | 93.26 |
| | 20% | 83.65 | 75.90 | 85.13 | 82.01 | 48.79 | 60.30 | 63.57 | 48.92 | 94.65 | 82.12 | 93.24 | 93.85 |
| | 40% | 83.72 | 76.03 | 85.25 | 82.25 | 49.01 | 60.89 | 64.01 | 49.04 | 94.66 | 82.24 | 93.46 | 93.79 |
| | 60% | 83.75 | 75.99 | 85.39 | 82.05 | 49.11 | 61.41 | 64.67 | 49.16 | 94.86 | 82.19 | 93.43 | 93.89 |
| | 80% | 83.67 | 75.89 | 85.50 | 82.27 | 48.88 | 61.33 | 64.53 | 49.28 | 94.67 | 82.23 | 93.42 | 93.93 |
| DeepLabv3+ + Monodepth2 | 0% | 80.01 | 66.77 | 80.72 | 77.15 | 51.67 | 54.15 | 60.41 | 48.07 | 93.35 | 76.69 | 91.45 | 92.86 |
| | 20% | 82.91 | 76.00 | 85.02 | 81.79 | 55.77 | 63.70 | 68.58 | 55.72 | 94.16 | 81.24 | 92.58 | 93.48 |
| | 40% | 83.12 | 76.23 | 84.98 | 82.18 | 56.19 | 64.44 | 69.25 | 56.14 | 94.21 | 81.36 | 92.69 | 93.59 |
| | 60% | 83.10 | 76.11 | 85.19 | 81.96 | 56.06 | 64.57 | 69.58 | 56.20 | 94.19 | 81.41 | 92.65 | 93.47 |
| | 80% | 83.03 | 75.94 | 85.15 | 81.68 | 56.11 | 64.50 | 69.65 | 56.39 | 94.17 | 81.31 | 92.50 | 93.49 |
| DualGCNet + BTS | 0% | 42.16 | 36.27 | 51.22 | 26.90 | 42.34 | 47.27 | 53.59 | 40.12 | 92.23 | 71.85 | 89.78 | 92.53 |
| | 20% | 82.59 | 74.59 | 83.06 | 80.56 | 45.76 | 56.88 | 60.12 | 45.48 | 94.71 | 81.85 | 92.56 | 93.79 |
| | 40% | 82.85 | 74.83 | 83.82 | 81.26 | 46.15 | 58.08 | 61.24 | 46.14 | 94.74 | 81.99 | 92.75 | 93.70 |
| | 60% | 82.82 | 74.72 | 83.58 | 81.20 | 46.19 | 58.15 | 61.26 | 46.39 | 94.71 | 81.85 | 92.73 | 93.77 |
| | 80% | 82.76 | 74.53 | 83.53 | 81.20 | 46.24 | 58.53 | 61.82 | 46.27 | 94.67 | 81.85 | 92.65 | 93.68 |
| DualGCNet + Monodepth2 | 0% | 49.03 | 39.01 | 57.26 | 19.29 | 47.92 | 49.11 | 57.06 | 44.16 | 92.39 | 73.17 | 89.82 | 92.23 |
| | 20% | 81.98 | 74.66 | 83.26 | 80.69 | 53.14 | 61.26 | 65.97 | 53.01 | 94.27 | 81.56 | 91.93 | 93.31 |
| | 40% | 82.27 | 74.97 | 83.28 | 81.02 | 53.77 | 62.30 | 66.95 | 53.61 | 94.39 | 81.60 | 92.02 | 93.51 |
| | 60% | 82.31 | 75.14 | 83.34 | 81.35 | 53.91 | 62.48 | 67.17 | 53.80 | 94.40 | 81.64 | 92.32 | 93.31 |
| | 80% | 82.06 | 74.42 | 82.91 | 80.82 | 53.76 | 62.59 | 67.21 | 53.73 | 94.34 | 81.54 | 91.96 | 93.47 |

TABLE IV

EVALUATION RESULTS OBTAINED BY DIFFERENT SPLITTINGS THAT ARE USED FOR FINE-TUNING THE META CLASSIFIER.

less accurate. On the other hand, these images motivate the benefit of our method as completely overlooked segments are detected. Furthermore, we bridge the domain shift in a post-processing manner that only requires two more inferences which run in parallel to semantic segmentation prediction.

c) *Fine-Tuning of the Meta Classifier*: Up to now, we have trained the segmentation networks as well as the meta classifier on Cityscapes for the experiments on A2D2, LostAndFound and IDD dataset. In this paragraph, we investigate the predictive power of the meta classifier and the implications on false negative reduction using parts of the target dataset for fine-tuning. Note, this domain adaptation only occurs in the post-processing meta classification step (retraining the neural networks is not necessary) and thus, the fine-tuning is lightweight and requires only a small amount of ground truth data. In detail, we retrain the meta classifier with 20%, 40%, 60% and 80% of the target dataset, respectively. The corresponding performance results are shown in Table IV. We observe great enhancements even with only a fine-tuning of 20% of the target domain obtaining an increase of up to 40.43 pp for $AUPRC$. The maximal increase is achieved for the A2D2 dataset (on the DualGCNet and BTS networks) for which 20% correspond to about 100 images that are used for retraining and achieving such an improvement. For all datasets, the greatest performance gap occurs between a trained meta classifier only on the Cityscapes dataset and using a small amount of the target domain data (here 20%). Increasing the subset of the target data, the performance is only slightly enhanced. Using

20% for fine-tuning, the highest $AUPRC$ value of 94.71% is obtained by the DualGCNet and the BTS network on the IDD dataset. The corresponding number of false positives and false negatives is given in Figure 3 (right). Note, the meta classifier for the baseline prediction is trained on the same train splitting. We outperform the basic semantic segmentation prediction and thus achieve a lower number of detection errors, in particular false negatives, therefore bridging the domain gap.

V. CONCLUSION AND OUTLOOK

In this work, we proposed a post-processing method to enhance the prediction of any semantic segmentation using monocular depth estimation. In particular, our approach reduce non-detected segments of a semantic segmentation network and bridge the domain gap given by different datasets with various objects and environments. To this end, we inferred a depth heatmap via a modified segmentation network that predicts foreground-background masks in parallel to a semantic segmentation network. Aggregating both predictions with a focus on foreground classes (here humans and vehicles) overlooked, i.e., false negative, segments are detected. To also minimize the false positives, meta classification as pruning step was applied based on uncertainty information. In our tests, we compared our method with the basic semantic segmentation prediction for several meta classification thresholds and improved the segment-wise precision and recall values. We obtained area under precision-recall curve values of up to 97.08% on source domain and up to 93.86% on target domain.

In conclusion, our approach performed well on the Cityscapes dataset (source domain) as well as on objects and environments not seen during training overcoming the domain shift.

As an extension of this work, it might be interesting to apply our method on other application fields like robotic navigation. In this case, a differentiation between foreground and background classes is possible, for example, the items in robotic navigation are most important. Our approach is applicable without major modifications, since trained depth estimation networks are available for several tasks and our modified segmentation network can be retrained on the same data like the basic semantic segmentation network uses. If a task-specific segmentation network is required, then as foreground-background network the semantic segmentation network architecture can be used only with small modifications on input and output.

ACKNOWLEDGMENT

We thank M. K. Neugebauer for support in data handling and programming. This work is supported by the Ministry of Culture and Science of the German state of North Rhine-Westphalia as part of the KI-Starter research funding program.

REFERENCES

- [1] L.-C. Chen, Y. Zhu, G. Papandreou *et al.*, “Encoder-decoder with atrous separable convolution for semantic image segmentation,” in *European Conference on Computer Vision (ECCV)*, 2018.
- [2] J. Wang, K. Sun, T. Cheng, B. Jiang, C. Deng, Y. Zhao, D. Liu, Y. Mu, M. Tan, X. Wang, W. Liu, and B. Xiao, “Deep high-resolution representation learning for visual recognition,” *IEEE Transactions on Pattern Analysis and Machine Intelligence*, 2021.
- [3] M. Cordts, M. Omran, S. Ramos *et al.*, “The cityscapes dataset for semantic urban scene understanding,” in *IEEE Conference on Computer Vision and Pattern Recognition (CVPR)*, 2016.
- [4] G. Varma, A. Subramanian, A. Namboodiri, M. Chandraker, and C. Jawahar, “IdD: A dataset for exploring problems of autonomous navigation in unconstrained environments,” in *IEEE Winter Conf. on Applications of Computer Vision (WACV)*, 2019.
- [5] K. Watanabe, K. Saito, Y. Ushiku, and T. Harada, “Multichannel semantic segmentation with unsupervised domain adaptation,” *European Conference on Computer Vision (ECCV) Workshop*, 2018.
- [6] Z.-Y. Shiao, W.-W. Lin, C.-S. Lin, and Y.-C. F. Wang, “Meta-learned feature critics for domain generalized semantic segmentation,” 2021.
- [7] S. Lee, H. Seong, S. Lee, and E. Kim, “Wildnet: Learning domain generalized semantic segmentation from the wild,” 2022.
- [8] E. H. Adelson, “On seeing stuff: the perception of materials by humans and machines,” in *IS&T/SPIE Electronic Imaging*, 2001.
- [9] A. Kirillov, K. He, R. Girshick, C. Rother, and P. Dollar, “Panoptic segmentation,” in *IEEE/CVF Conference on Computer Vision and Pattern Recognition (CVPR)*, 2019.
- [10] P. Pinggera, S. Ramos, S. Gehrig, U. Franke, C. Rother, and R. Mester, “Lost and found: detecting small road hazards for self-driving vehicles,” in *IEEE/RSJ International Conference on Intelligent Robots and Systems (IROS)*, 2016.
- [11] M. Rottmann, P. Colling, T. Hack, F. Hüger, P. Schlicht *et al.*, “Prediction error meta classification in semantic segmentation: Detection via aggregated dispersion measures of softmax probabilities,” in *IEEE International Joint Conference on Neural Networks (IJCNN) 2020*, 2020.
- [12] K. Maag, M. Rottmann, and H. Gottschalk, “Time-dynamic estimates of the reliability of deep semantic segmentation networks,” in *IEEE International Conference on Tools with Artificial Intelligence (ICTAI)*, 2020.
- [13] K. Maag, M. Rottmann, S. Varghese, F. Hüger, P. Schlicht, and H. Gottschalk, “Improving video instance segmentation by light-weight temporal uncertainty estimates,” in *International Joint Conference on Neural Network (IJCNN)*, 2021.
- [14] P. Jaccard, “The distribution of the flora in the alpine zone,” *New Phytologist*, 1912.
- [15] R. Chan, M. Rottmann, F. Hüger, P. Schlicht, and H. Gottschalk, “Metafusion: Controlled false-negative reduction of minority classes in semantic segmentation,” *IEEE International Joint Conference on Neural Networks (IJCNN)*, 2020.
- [16] K. Maag, “False negative reduction in video instance segmentation using uncertainty estimates,” in *IEEE International Conference on Tools with Artificial Intelligence (ICTAI)*, 2021.
- [17] L. Zhang, X. Li, A. Arnab, K. Yang, Y. Tong, and P. H. Torr, “Dual graph convolutional network for semantic segmentation,” in *British Machine Vision Conference (BMVC)*, 2019.
- [18] C. Godard, O. Mac Aodha, M. Firman, and G. J. Brostow, “Digging into self-supervised monocular depth prediction,” 2019.
- [19] J. H. Lee, M.-K. Han, D. W. Ko, and I. H. Suh, “From big to small: Multi-scale local planar guidance for monocular depth estimation,” 2019.
- [20] J. Geyer, Y. Kassahun, M. Mahmudi, X. Ricou, R. Durgesh, A. S. Chung, L. Hauswald, V. H. Pham, M. Mühlegg, S. Dorn, T. Fernandez, M. Janicke, S. Mirashi, C. Savani, M. Sturm, O. Vorobiov, M. Oelker, S. Garreis, and P. Schuberth, “A2D2: Audi Autonomous Driving Dataset,” 2020.
- [21] W. Yan, Y. Wang, S. Gu, L. Huang, F. Yan, L. Xia, and Q. Tao, “The domain shift problem of medical image segmentation and vendor-adaptation by unet-gan,” *Medical Image Computing and Computer Assisted Intervention*, 2019.
- [22] A. Cardace, L. Luigi, P. Zama Ramirez, S. Salti, and L. Di Stefano, “Plugging self-supervised monocular depth into unsupervised domain adaptation for semantic segmentation,” 2022.
- [23] Q. Wang, D. Dai, L. Hoyer, L. Van Gool, and O. Fink, “Domain adaptive semantic segmentation with self-supervised depth estimation,” in *IEEE/CVF International Conference on Computer Vision (ICCV)*, 2021.
- [24] W. Chen, Z. Yu, Z. Wang, and A. Anandkumar, “Automated synthetic-to-real generalization,” in *International Conference on Machine Learning (ICML)*, 2020.
- [25] Y. Zhao, Z. Zhong, N. Zhao, N. Sebe, and G. H. Lee, “Style-hallucinated dual consistency learning for domain generalized semantic segmentation,” 2022.
- [26] N. Kim, T. Son, C. Lan, W. Zeng, and S. Kwak, “Wedge: Web-image assisted domain generalization for semantic segmentation,” 09 2021.
- [27] S. Choi, S. Jung, H. Yun, J. T. Kim, S. Kim, and J. Choo, “Robustnet: Improving domain generalization in urban-scene segmentation via instance selective whitening,” *IEEE/CVF Conference on Computer Vision and Pattern Recognition (CVPR)*, pp. 11 575–11 585, 2021.
- [28] K. Xiang, K. Wang, and K. Yang, “A comparative study of high-recall real-time semantic segmentation based on swift factorized network,” *Security + Defence*, 2019.
- [29] K. Xiang, K. Wang, and K. Yang, “Importance-aware semantic segmentation with efficient pyramidal context network for navigational assistant systems,” *IEEE Intelligent Transportation Systems Conference (ITSC)*, 2019.
- [30] J. Tian, N. C. Mithun, Z. Seymour, H. Chiu, and Z. Kira, “Striking the right balance: Recall loss for semantic segmentation,” 2021.
- [31] Y. Zhong, B. Yuan, H. Wu, Z. Yuan, J. Peng, and Y.-X. Wang, “Pixel contrastive-consistent semi-supervised semantic segmentation,” in *IEEE/CVF International Conference on Computer Vision (ICCV)*, 2021.
- [32] P.-Y. Chen, A. H. Liu, Y.-C. Liu, and Y.-C. F. Wang, “Towards scene understanding: Unsupervised monocular depth estimation with semantic-aware representation,” in *IEEE/CVF Conference on Computer Vision and Pattern Recognition (CVPR)*, 2019.
- [33] J. Jiao, Y. Cao, Y. Song, and R. Lau, “Look deeper into depth: Monocular depth estimation with semantic booster and attention-driven loss,” in *European Conference on Computer Vision (ECCV)*, 2018.
- [34] C. Hazirbas, L. Ma, C. Domokos, and D. Cremers, “Fusenet: Incorporating depth into semantic segmentation via fusion-based cnn architecture,” in *Asian Conference on Computer Vision (ACCV)*, 2016.
- [35] Y. Cao, C. Shen, and H. T. Shen, “Exploiting depth from single monocular images for object detection and semantic segmentation,” *IEEE Transactions on Image Processing*, 2017.
- [36] J. Novosel, “Boosting semantic segmentation with multi-task self-supervised learning for autonomous driving applications,” 2019.
- [37] H. Jiang, G. Larsson, M. Maire, G. Shakhnarovich, and E. G. Learned-Miller, “Self-supervised relative depth learning for urban scene understanding,” in *European Conference on Computer Vision (ECCV)*, 2018.

- [38] L. Hoyer, D. Dai, Y. Chen, A. Koring, S. Saha, and L. Gool, “Three ways to improve semantic segmentation with self-supervised depth estimation,” 2021.
- [39] J. H. Friedman, “Stochastic gradient boosting,” *Comput. Stat. Data Anal.*, 2002.
- [40] Z. Wu, C. Shen, and A. Hengel, “Wider or deeper: Revisiting the resnet model for visual recognition,” *Pattern Recognition*, 2016.
- [41] K. He, X. Zhang, S. Ren, and J. Sun, “Deep residual learning for image recognition,” 2016.
- [42] A. Geiger, P. Lenz, C. Stiller, and R. Urtasun, “Vision meets robotics: The kitti dataset,” *The International Journal of Robotics Research*, 2013.
- [43] G. Huang, Z. Liu, and K. Q. Weinberger, “Densely connected convolutional networks,” *IEEE Conference on Computer Vision and Pattern Recognition (CVPR)*, 2017.

APPENDIX A DETAILS ON META CLASSIFICATION

The semantic segmentation neural network provides for each pixel z a probability distribution $f_z(y|x)$ over a label space $\mathcal{C} = \{y_1, \dots, y_c\}$, with $y \in \mathcal{C}$ and given an input image x . The degree of randomness in semantic segmentation prediction is quantified by (pixel-wise) dispersion measures, such as the entropy

$$E_z(x) = -\frac{1}{\log(c)} \sum_{y \in \mathcal{C}} f_z(y|x) \log f_z(y|x), \quad (3)$$

(see Figure 5 (right)) the variation ratio

$$V_z = 1 - f_z(\hat{y}_z(x)|x) \quad (4)$$

or the probability margin

$$M_z(x) = V_z + \max_{y \in \mathcal{C} \setminus \{\hat{y}_z(x)\}} f_z(y|x) \quad (5)$$

with predicted class

$$\hat{y}_z(x) = \arg \max_{y \in \mathcal{C}} f_z(y|x). \quad (6)$$

Based on the different behavior of these measures and the segment’s geometry for correct and false predictions, we construct segment-wise features by hand to quantify the observations that we made. Let $\hat{\mathcal{P}}_x$ denote the set of predicted segments, i.e., connected components, (of the foreground class). By aggregating these pixel-wise measures, segment-wise features are obtained and serve as input for the meta classifier. To this end, we compute for each segment $q \in \hat{\mathcal{P}}_x$ the mean of the pixel-wise uncertainty values of a given segment, i.e., *mean dispersions* \bar{D} , $D \in \{E, V, M\}$. Furthermore, we distinguish between the *inner* of the segment $q_{in} \subset q$ consisting of all pixels whose eight neighboring pixels are also elements of q and the *boundary* $q_{bd} = q \setminus q_{in}$. We observe that poor or false predictions are often accompanied by fractal segment shapes (a relatively large amount of boundary pixels). An example is shown in Figure 5 (left). This results in *segment size* $S = |q|$ and mean dispersion features per segment also for the inner and the boundary since uncertainties may be higher on a segment’s boundary (see Figure 5 (right)). Additionally, we define *relative segment sizes* $\tilde{S} = S/S_{bd}$ and $\tilde{S}_{in} = S_{in}/S_{bd}$ quantifying the degree of fractality as well as *relative mean dispersions* $\tilde{D} = \bar{D}\tilde{S}$ and $\tilde{D}_{in} = \bar{D}_{in}\tilde{S}_{in}$ where $D \in \{E, V, M\}$.

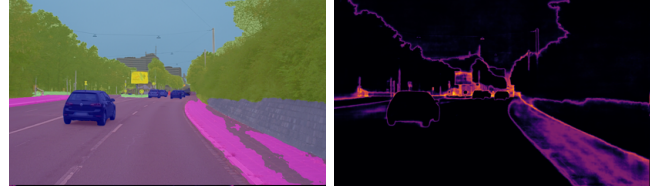


Fig. 5. *Left*: Semantic segmentation predicted by a DNN. *Right*: Entropy heatmap.

For the foreground-background segmentation, given the same input image x , we obtain for each pixel z the probability of being a foreground pixel $g_z(x) \in [0, 1]$. Thus, we calculate the mean and relative entropy features for the foreground-background prediction (having only two classes), denoted by \bar{F}_* , $*$ $\in \{_, in, bd\}$, \tilde{F} and \tilde{F}_{in} . Last, we add the *geometric center*

$$\bar{q} = \frac{1}{S} \sum_{(z_v, z_h) \in q} (z_v, z_h) \quad (7)$$

where (z_v, z_h) describes the vertical and horizontal coordinate of pixel z and the *mean class probabilities*

$$P(y|q) = \frac{1}{S} \sum_{z \in q} f_z(y|x) \quad (8)$$

for each foreground class $y \in \tilde{\mathcal{C}} \subset \mathcal{C}$ where $\tilde{\mathcal{C}} = \{y_1, \dots, y_{\tilde{c}}\}$, $\tilde{c} < c$, to our set of hand-crafted features, resulting in the following set:

$$U^q = \{\bar{D}, \bar{D}_{in}, \bar{D}_{bd}, \tilde{D}, \tilde{D}_{in} : D \in \{E, V, M, F\}\} \cup \{\bar{q}\} \cup \{S, S_{in}, S_{bd}, \tilde{S}, \tilde{S}_{in}\} \cup \{P(y|q) : y \in \tilde{\mathcal{C}}\}. \quad (9)$$

Analogously to the set of predicted segments $\hat{\mathcal{P}}_x$, we denote by \mathcal{P}_x the set of segments in the ground truth \mathcal{S}_x . To determine if a predicted segment $q \in \hat{\mathcal{P}}_x$ is a false positive, we consider the intersection over union. The segment-wise *IoU* is then defined as

$$IoU(q) = \frac{|q \cap Q|}{|q \cup Q|}, \quad Q = \bigcup_{q' \in \mathcal{P}_x, q' \cap q \neq \emptyset} q'. \quad (10)$$

APPENDIX B MORE DETAILS ON EVALUATION METRICS

Let $\hat{\mathcal{P}}_x$ denote the set of predicted segments and \mathcal{P}_x of ground truth segments. Meta classification provides a probability $m(q) \in [0, 1]$ for each segment $q \in \hat{\mathcal{P}}_x$ to be a false positive on which we threshold with different values $h \in H = \{0.00, 0.01, \dots, 0.99, 1.00\}$. A predicted false positive segment is considered as background. For each threshold h , we calculate over all foreground segments in a given validation set \mathcal{X} the number of false positives

$$FP(h) = \sum_{x \in \mathcal{X}} \sum_{q \in \hat{\mathcal{P}}_x} 1_{\{IoU(q)=0\}} 1_{\{m(q) \leq h\}}, \quad (11)$$

true positives

$$TP(h) = \sum_{x \in \mathcal{X}} \sum_{q' \in \mathcal{P}_x} 1_{\{IoU'(q, h) > 0\}} \quad (12)$$

and false negatives

$$FN(h) = \sum_{x \in \mathcal{X}} \sum_{q' \in \mathcal{P}_x} 1_{\{IoU'(q, h) = 0\}} \quad (13)$$

where the indicator function is defined as

$$1_{\{A\}} = \begin{cases} 1, & \text{if event } A \text{ happens} \\ 0, & \text{else} \end{cases} \quad (14)$$

and the IoU for a ground truth segment $q' \in \mathcal{P}_x$ as

$$IoU'(q', h) = \frac{|q' \cap Q'|}{|q' \cup Q'|}, \quad Q' = \bigcup_{\substack{q \in \hat{\mathcal{P}}_x, q \cap q' \neq \emptyset \\ m(q) \leq h}} q. \quad (15)$$

Thus, we obtain precision

$$prec(h) = \frac{TP(h)}{TP(h) + FP(h)} \quad (16)$$

and recall

$$rec(h) = \frac{TP(h)}{TP(h) + FN(h)} \quad (17)$$

values on segment-level dependent of h . The degree of separability is then computed as the area under precision recall curve ($AUPRC$) by thresholding the meta classification probability. Furthermore, we use the recall rate at 80% precision rate (REC_{80}) for the evaluation. Moreover, we consider the segment-wise F_1 score which is defined by

$$F_1(h) = 2 \cdot \frac{prec(h) \cdot rec(h)}{prec(h) + rec(h)}. \quad (18)$$

To obtain an evaluation metric independent of the meta classification threshold h , we calculate the averaged F_1 score

$$\bar{F}_1 = \frac{1}{|H|} \sum_{h \in H} F_1(h) \quad (19)$$

and the optimal F_1 score

$$F_1^* = \max_{h \in H} F_1(h). \quad (20)$$

meta classification. Noteworthy, the F_1 score for the basic semantic segmentation performance is also enhanced by up to 39.59 pp. Moreover, the results show that without using meta classification the basic semantic segmentation prediction outperforms our method. This is caused by our foreground-background segmentation based on depth estimation being more prone to predicting foreground segments. We produce more possible foreground segments to reduce false negatives and using the false positive pruning, we outperform basic semantic segmentation.

APPENDIX D

NUMERICAL RESULTS PER CLASS

Up to now, the given results have been aggregated for all foreground classes, here we present results for three foreground classes separately, i.e., person, car and bicycle, see [Table VI](#), [Table VII](#) and [Table VIII](#), respectively. As the LostAndFound dataset provides only labels for road and small obstacles, a class-wise evaluation is not possible. In most cases, we outperform the basic semantic segmentation prediction, although differences for the datasets and the three classes are observed. The highest performance up to 89.20% $AUPRC$ is achieved for Cityscapes since this is the source domain and thus, the semantic segmentation network produces strong predictions. Under domain shift, we obtain $AUPRC$ values of up to 75.53%. As for the foreground classes in general, there is no clear tendency which depth estimation network used in our method performs better. For the class car, we achieve higher performance metrics in comparison to classes person and bicycle. Cars occur more frequently than persons and bicycles in all three datasets (see [\[3\]](#), [\[4\]](#), [\[20\]](#)) and are easier to recognize given their larger size and similar shape. In summary, we improve the detection performance of the basic semantic segmentation network in most cases and in particular, bridge the domain gap. Even though our performance for bicycles, for example, is comparatively lower, we generally detect more overlooked foreground segments and thus, reduce false negatives.

APPENDIX C

EFFECTS OF META CLASSIFICATION

In [Table V](#), we show the effects of meta classification comparing the F_1 score (see [Equation 18](#)) performance with and without meta classification. $F_1(1)$ corresponds to the obtained precision and recall values without post-processing, i.e., meta classification and F_1^* to the best possible ratio of both rates. Note, we use the meta classifier trained only on the source domain dataset Cityscapes. We observe that false positive pruning significantly improves the performance of our method as many false positive segments are predicted by the aggregation step to reduce the number of false negatives. We increase the F_1 score of up to 65.72 pp for our method using

| | Cityscapes | | | A2D2 | | LostAndFound | | IDD | |
|--------------|--------------|--------------|--|--------------|--------------|--------------|--------------|--------------|--------------|
| | $F_1(1)$ | F_1^* | | $F_1(1)$ | F_1^* | $F_1(1)$ | F_1^* | $F_1(1)$ | F_1^* |
| DeepLabv3+ | 84.00 | 94.69 | | 52.16 | 76.36 | 49.54 | 53.06 | 69.14 | 87.79 |
| + BTS | 43.16 | 95.80 | | 25.09 | 80.46 | 40.19 | 57.80 | 39.00 | 91.75 |
| + Monodepth2 | 38.11 | 95.73 | | 17.16 | 80.72 | 33.61 | 60.41 | 25.73 | 91.45 |
| DualGCNet | 82.82 | 92.77 | | 25.89 | 65.48 | 45.88 | 50.21 | 64.11 | 87.37 |
| + BTS | 53.99 | 94.66 | | 25.40 | 51.22 | 40.17 | 53.59 | 44.64 | 89.78 |
| + Monodepth2 | 50.92 | 94.58 | | 23.98 | 57.26 | 35.07 | 57.06 | 35.87 | 89.82 |

TABLE V

EVALUATION RESULTS USING META CLASSIFICATION (F_1^*) AND WITHOUT ($F_1(1)$) FOR THE BASIC SEMANTIC SEGMENTATION PREDICTION (DEEPLABV3+/DUALGCNET) AND OUR APPROACH, I.E., THE DEEPLABV3+/DUALGCNET PREDICTION AGGREGATED WITH FOREGROUND-BACKGROUND PREDICTION USING BTS OR MONODEPTH2.

| | Cityscapes | | | A2D2 | | | IDD | | |
|--------------|--------------|--------------|--------------|--------------|--------------|--------------|--------------|--------------|--------------|
| | <i>AUPRC</i> | \bar{F}_1 | F_1^* | <i>AUPRC</i> | \bar{F}_1 | F_1^* | <i>AUPRC</i> | \bar{F}_1 | F_1^* |
| DeepLabv3+ | 83.11 | 80.33 | 84.66 | 40.66 | 40.19 | 54.83 | 39.70 | 35.31 | 56.78 |
| + BTS | 87.36 | 80.36 | 86.89 | 47.10 | 43.37 | 55.43 | 46.14 | 41.05 | 54.94 |
| + Monodepth2 | 86.87 | 80.27 | 86.62 | 48.85 | 41.83 | 56.60 | 48.88 | 40.73 | 56.80 |
| DualGCNet | 75.05 | 73.30 | 77.12 | 13.67 | 17.64 | 35.34 | 31.29 | 25.37 | 47.28 |
| + BTS | 79.72 | 73.24 | 80.30 | 13.28 | 20.68 | 28.42 | 36.94 | 30.23 | 47.72 |
| + Monodepth2 | 78.39 | 72.78 | 79.70 | 13.56 | 21.28 | 28.61 | 41.51 | 31.48 | 48.08 |

TABLE VI

PERFORMANCE RESULTS FOR THE BASIC SEMANTIC SEGMENTATION PREDICTION (DEEPLABV3+/DUALGCNET) VS. OUR APPROACH, I.E., THE DEEPLABV3+/DUALGCNET PREDICTION AGGREGATED WITH FOREGROUND-BACKGROUND PREDICTION USING BTS OR MONODEPTH2, FOR CLASS PERSON.

| | Cityscapes | | | A2D2 | | | IDD | | |
|--------------|--------------|--------------|--------------|--------------|--------------|--------------|--------------|--------------|--------------|
| | <i>AUPRC</i> | \bar{F}_1 | F_1^* | <i>AUPRC</i> | \bar{F}_1 | F_1^* | <i>AUPRC</i> | \bar{F}_1 | F_1^* |
| DeepLabv3+ | 86.19 | 85.18 | 89.31 | 64.77 | 56.21 | 73.16 | 55.25 | 39.92 | 70.03 |
| + BTS | 89.20 | 85.69 | 90.61 | 75.53 | 66.74 | 77.44 | 69.99 | 50.97 | 73.45 |
| + Monodepth2 | 88.83 | 85.15 | 90.20 | 74.82 | 67.26 | 77.45 | 68.03 | 49.70 | 72.59 |
| DualGCNet | 81.76 | 81.45 | 85.44 | 39.65 | 21.93 | 59.85 | 57.28 | 41.89 | 69.07 |
| + BTS | 85.88 | 81.31 | 87.39 | 33.52 | 30.37 | 46.14 | 63.12 | 46.67 | 69.70 |
| + Monodepth2 | 85.24 | 81.24 | 87.13 | 40.63 | 34.00 | 53.89 | 64.52 | 48.50 | 69.93 |

TABLE VII

PERFORMANCE RESULTS FOR THE BASIC SEMANTIC SEGMENTATION PREDICTION VS. OUR APPROACH FOR CLASS CAR.

| | Cityscapes | | | A2D2 | | | IDD | | |
|--------------|--------------|--------------|--------------|--------------|--------------|--------------|--------------|--------------|--------------|
| | <i>AUPRC</i> | \bar{F}_1 | F_1^* | <i>AUPRC</i> | \bar{F}_1 | F_1^* | <i>AUPRC</i> | \bar{F}_1 | F_1^* |
| DeepLabv3+ | 85.46 | 80.25 | 87.43 | 37.37 | 47.00 | 49.67 | 14.36 | 9.73 | 33.73 |
| + BTS | 86.99 | 79.02 | 86.64 | 43.78 | 48.47 | 54.88 | 21.70 | 13.70 | 38.25 |
| + Monodepth2 | 87.20 | 78.54 | 86.93 | 42.37 | 46.97 | 53.24 | 23.78 | 13.79 | 39.84 |
| DualGCNet | 77.05 | 73.43 | 80.62 | 15.22 | 19.85 | 27.27 | 16.06 | 8.68 | 36.79 |
| + BTS | 79.49 | 72.68 | 81.16 | 8.08 | 21.30 | 23.08 | 16.00 | 9.56 | 33.51 |
| + Monodepth2 | 79.99 | 72.82 | 81.93 | 10.23 | 19.70 | 21.28 | 21.93 | 10.70 | 36.36 |

TABLE VIII

PERFORMANCE RESULTS FOR THE BASIC SEMANTIC SEGMENTATION PREDICTION VS. OUR APPROACH FOR CLASS BICYCLE.